Bone and cartilage differentiation of a single stem cell population driven by material interface.

Author names

Hannah Donnelly[1], Carol-Anne Smith[1], Paula E Sweeten[1], Nikolaj Gadegaard[2], R.M. Dominic Meek[3], Matteo D'Este[4], Alvaro Mata[5,6], David Eglin[4], Matthew J Dalby[1]

Affiliations:

[1]Centre for Cell Engineering, University of Glasgow, Glasgow, U.K.

[2]Division of Biomedical Engineering, University of Glasgow, Glasgow, U.K.,

[3]Department of Orthopaedics, Southern General Hospital, Glasgow, U.K.

[4]AO Research Institute Davos, Davos, Switzerland

[5]Institute of Bioengineering, Queen Mary University of London, London, U.K.

[6]School of Engineering and Materials Science, Queen Mary University of London, London, U.K.

Corresponding author:

Hannah Donnelly, Centre for Cell Engineering, University of Glasgow, Joseph Black Building, University of Glasgow, Glasgow, G12 8QQ, U.K.

Email: H.donnelly.1@research.gla.ac.uk

Abstract

Adult stem cells, such as mesenchymal stem cells, are a multipotent cell source able to differentiate toward multiple cell types. While used widely in tissue engineering and biomaterials research, they present inherent donor variability and functionalities. In addition, their potential to form multiple tissues is rarely exploited. Here we combine an osteogenic nanotopography and a chondrogenic hyaluronan hydrogel with the hypothesis

that we can make a complex tissue from a single multipotent cell source with the exemplar of creating a 3D bone-cartilage boundary environment. MSCs were seeded onto the topographical surface and the temperature gelling hydrogel laid on top. Cells that remained on the nanotopography spread and formed osteoblast-like cells while those that were seeded into or migrated into the gel remained rounded and expressed chondrogenic markers. This novel, simple interfacial environment provides a platform for anisotropic differentiation of cells from a single source, which could ultimately be exploited to sort osteogenic and chondrogenic progenitor cells from a MSC population and to develop a tissue engineered interface.

Introduction

Articular cartilage, found at the surface ends of long bones, is an avascular, aneural connective tissue with a functional capacity to dissipate biomechanical loads and allow smooth articulation of joints.[1] At the macroscopic level it contains just one functional cell type, the chondrocyte. The cells regulate, synthesise and assemble a complex extracellular matrix (ECM) during the chondroblastic stage before terminally differentiating to the chondrocyte to maintain the tissue. However, due to the avascular nature of the tissue, repair is highly limited after injury and degradation is mainly irreversible leading to osteoarthritis (OA) which is a degenerative and disabling joint disease.

One of the main issues in repair of articular cartilage injury is that it often involves two tissues, bone and cartilage at their interface. Current treatments involving chondrocyte implantation to the defected site do not address the importance of the interface with the subchondral bone. Microfracture technique consisting in mobilising cells from the bony region tends to be suboptimal in term of cartilage tissue formation.

Thus, use of stem cells, particularly skeletal marrow stromal cells (MSCs) capable of forming both cartilage and bone, may be desirable as: (a) they have high proliferative capacity and (b) their use would allow complex and interfacial tissue engineering (i.e.

forming bone and cartilage) from a single cell type. However, distinct environmental cues are required to support differentiation down the desired osteo- or chondro- lineage of the MSCs. We note that while stem cells, particularly, MSCs are widely used in biomaterials and tissue engineering research, achieving spatial positioning of different cell types from a single cell source within a scaffold is challenging as different cell cues are required in different locations. Such cues can be physical (chemistry of the scaffold/grafting of chemistry, stiffness control, topographical information[2–7]), biological (i.e. peptides, growth factors[8]), or a combination of both.[9,10] Growth factors have been added with spatial control to direct multiple stem cells fates.[11,12] Similarly, plasmids were spatially delivered through a bilayer structure for the differentiation of MSCs toward bone and cartilage.[13] While the use of a biphasic scaffold is not novel[14] the self-organisation of hMSCs capabilities on designed scaffolds in basal media is both desirable and novel.

In this study we employed an osteogenic nanoscale topography[6] embossed on a biodegradable, poly(ε-caprolactone) (PCL) membrane and a hyaluronan hydrogel capable of supporting chondrogenesis.[15] This modular system is designed to permit osteogenesis at the topography/gel interface and chondrogenesis within the gel using a multipotential, but critically single cell type source, MSCs, in the absence of directing external biological cues.

Materials and Methods

Generation of FLAT and NSQ surfaces

As previously described, quartz slides of near-square (NSQ) topography (120nm pits in square arrangement, centre–centre spacing of 300 nm, with ±50 nm offset in pit

placement in x and y axes [4,6]) and glass coverslips of FLAT topography were used to create multiple polymer replicas by manual hot (80°C) embossing poly(ε-caprolactone) beads ($(C_6H_{10}O_2)n$; PCL (Sigma Aldrich): typical disks 13 mm in diameter, suitable for cell culture in 24 well plates. PCL disks were treated for 30 seconds at MHz-range Radio Frequency (RF) in a plasma cleaner (PDC-002 Harrick Plasma) to remove organic contaminants and activate the surface to improve cell surface attachment, then sterilized in 70% ethanol for 30 minutes and two sequential 5 minute washes in cell culture media prior to cell seeding.

Synthesis of poly(N-isopropylacrylamide) hyaluronan derivative.

The derivative was prepared as already reported.[16] Briefly, amino-terminated poly(*N*-isopropylacrylamide) (PNIPAM-NH_2) was synthesized by dissolving 10 g of *N*-isopropylacrylamide in 20 ml of dry *N,N*-dimethylformamide (DMF). Under nitrogen atmosphere, 15 mg of azobisisobutyronitrile and 30 mg of cysteamine hydrochloride were added, and the reaction was let to proceed for 6 hrs. The product was precipitated and washed with diethyl ether. The PNIPAM-NH_2 M_w value was 40'300 $g \cdot mol^{-1}$ as measured by gel permeation chromatography. HA sodium salt from *Streptococcus equi* (HANa) with M_w of 293'000 $g.mol^{-1}$ and polydispersity PDI = 1.86 (Contipro Biotech.) was transformed in its tetrabutylammonium salt (HATBA) via cationic exchange. Then, 2.0 g of HATBA were dissolved in 200 ml of dry dimethyl sulfoxide at RT. Methanesulfonic acid and 1,1'-carbonyldiimidazole both equimolar to the repeating unit of HA were added and 3.7 g of PNIPAM-NH_2 added and stirred at RT for 3 days. The solution was dialysed against demineralized water using regenerated cellulose dialysis tubes (MWCO 50 kDa) for 5 days and finally freeze dried. ^1H NMR analysis was

performed on a Bruker Avance AV-500 NMR spectrometer using deuterium oxide as solvent to assess the degree of grafting of pNIPAM-NH_2 onto HA.

Reconstitution and rheology of thermoresponsive hyaluronan solution.

The hyaluronan derivative was reconstituted to 15% w:v in sterile phosphate buffered saline (PBS) and stored at 4°C for 24 hrs for complete dissolution. Rheological measurements were performed on an Anton Paar MCR-302 rheometer equipped with Peltier temperature control device and thermostatic hood. A 1° conical geometry of 25 mm diameter and 49 µm gap was used. For each sample an amplitude sweep was measured at 10 rad/s and 37.00 ± 0.03 °C. Storage moduli were measured as function of the temperature between 20 °C and 40 °C with a gradient of 1 °C/min at angular frequency of 10 rad/s and amplitude within the linear viscoelastic range. A thin layer of low-viscosity silicon oil was spread along the meniscus interface in order to avoid evaporation.

Cell isolation and culture.

MSCs were isolated from haematologically normal patients undergoing routine surgery as previously described.[17] MSCs were cultured in growth media containing 86% DMEM (Sigma) supplemented with 10% Fetal Bovine Serum (FBS) (Sigma, UK), 2% penicillin streptomycin, 1% non-essential amino acids (Invitrogen, UK) and 1% 100mM sodium pyruvate (Life Technologies, UK) at 37°C with a 5% CO_2 atmosphere. Media was changed every 3 days and cells passaged to passage 2 or 3. hMSCs were seeded on NQS topography PCL surfaces in 24 well plates at 1 x 10^4 cells per PCL disk (surface area of disk average 1.13 cm^2), media as recipe above and incubated for 24 hours to allow for

adherence. Then, 250 µL of 1 x 10^4 cells/ml of thermoresponsive hyaluronan composition at temperature around 10°C was added and allowed to flow on top of the PCL disk before incubation at 37°C for 10 – 15 minutes to allow gelation, resultant gel approximately 0.5 cm thickness. 13 mm glass coverslips sterilized in 70% ethanol were subsequently added on top to ensure that the hydrogel was always in contact with the underlying PCL disk. Note that MSCs from Promocell were used to generate Supplementary Figure 1.

Immunocytochemistry.

After 5 days of culture, cells were fixed (10 ml 37% formaldehyde, 2g sucrose in 90 ml PBS solution) for 15 minutes. Permeabilising buffer (10.3g sucrose, 0.292g NaCl, 0.06g $MgCl_2$, 0.476g HEPES, 0.5 ml Triton X, in 100 ml of H_2O, at pH 7.2) was then added for 15 minutes to control samples without hydrogel (-GEL), and for 2 hours to samples with hydrogel (+GEL). To block non-specific binding samples were incubated in 1% BSA/PBS for 15 min -GEL, and 1 hour +GEL. Primary antibodies (1:50 in 1% BSA/PBS) were added at 200 µL/well for 1 hour -GEL, and at 500 µl/well overnight (+GEL). Substrates were then washed three times in 0.5% Tween 20/PBS (5 minutes each –GEL, 20 minutes each +GEL). Corresponding secondary biotin-conjugated antibody (1:50 in 1% BSA/PBS) was added for 3 hours to –GEL and +GEL samples, followed by substrate washing as described above. FITC-conjugated streptavidin was added (1:50 in 1% BSA/PBS, Vector Laboratories) for 2 hours before samples were given a final wash. All immunostaining were carried out at 37°C with warmed solutions in order to maintain hydrogel integrity. Surfaces were mounted using mounting medium for fluorescence, with DAPI counterstain (Vector Laboratories, UK), and viewed by

fluorescent microscopy (Zeiss Axiophot). Digital images were captured in two fluorescent channels (x20 magnification) and saved for further processing. Primary antibodies presented in Table 1. Secondary antibodies: biotinylated monoclonal anti-mouse (IgG) raised in horse and fluorescein streptavidin (all Vector Laboratories, UK).

Table 1. Table of primary antibodies used for immunocytochemistry.

Target Molecule	Host	Isotype	Source	Reference
β3 Tubulin	mouse	Monoclonal, IgG2b	Sigma, UK	[18–20]
Phosphorylated RUNX2	mouse	Monoclonal, IgG2a	Abcam, UK	[21,22]
Vinculin	mouse	hVIN-1, Monoclonal, IgG1	Sigma, UK	[5,20,23,24]
SOX9	mouse	Monoclonal, IgG2a	Abcam, UK	[25,26]
Osteocalcin	mouse	Monoclonal, IgG2a	Santa Cruz Biotechnology, USA	[23,27]

Von Kossa staining.

After 28 days of culture, cells were fixed for 15 minutes in 4% formaldehyde solution and stored in PBS overnight. 1 ml of 5% silver nitrate solution (5g silver nitrate, 100ml deionized H_2O, kept in dark) was added to each sample well and exposed to U.V. light for 20 minutes. Samples were washed thrice in deionized water. 1 ml 5% sodium thiosulphate solution (5g sodium thiosulphate, 100ml deionized H_2O, stored in dark) was added for 10 minutes, samples were washed as described above. 1 ml counterstain solution (0.1g nuclear fast red, 5g aluminium sulphate in 100ml deionized H_2O, boiled for 5 minutes and filtered) was added for 3 minutes. Samples were washed as described above and finally rinsed in 70% ethanol. Digital images of PCL disks were captured and saved for further analysis. The whole procedure was carried out at 37°C to maintain gel integrity. The hydrogel was washed away during the staining protocol and therefore is not imaged.

Quantitative PCR.

Samples were harvested after 28 days of culture in triplicate by transferring hydrogels to a 2 ml Eppendorf tube and adding 1 ml of TRIZOL reagent and incubating at room temperature for 10 mins. Cells on PCL substrates were removed by trypsinization and cell pellet was added to corresponding hydrogel TRIZOL solution. Samples were stored at -80 °C until RNA isolation. RNA was isolated using RNAeasy micro kit according to manufacturer protocol (Qiagen, UK). RNA pellets were solubilized in RNase free water and assessed for concentration and purity with measured absorbance at 230 nm, 260 nm (nucleic acids) using a NanoDrop ND 100 spectrometer (Thermo Scientific). Reverse transcription was carried out on extracted RNA using an Omniscript Reverse Transcription kit (Qiagen, UK) according to manufacturer's instructions, with Random Primers (Invitrogen, UK) and RNAsin (Promega, USA). Quantitative PCR was carried out using a qPCR detection system (model 7500, Applied Biosciences) by the SYBR green method. Expression of SOX9 (Table 2) were tested, and GAPDH expression was used as a reference gene to normalize all data. RQ (relative gene expression) values were automatically calculated by the delta delta CT method. Statistical analysis first determined that GAPDH did not vary under test conditions (one-way ANOVA;). Cycle threshold values were then converted from logarithmic to linear scale ($2^{\Delta\Delta\text{-CT}}$) for further analysis.

Table 2. Primers used for qPCR

PRIMER	FORWARD	REVERSE
GAPDH	TCAAGGCTGAGAACGGGAA	TGGGTGGCAGTGATGGCA
SOX9	AGACAGCCCCCTATCGACTT	CGGCAGGTACTGGTCAAACT

Statistical Analysis.

For analysis of gene expression the $2^{\Delta\Delta\text{-}C}{}_T$ method was used.[28] Statistical analysis was carried out using the Tukey Kramer multiple-comparisons post-test analysis of variance (ANOVA). Relative transcript levels expressed as the mean ± standard deviation for plotting on graphs. (n=3 for each condition).

Results

Unless stated, experiments were set up as depicted in the scheme in Figure 1, with MSCs seeded onto the flat control or NSQ nanotopographical for 24 hrs before setting the gel on top of the cells.

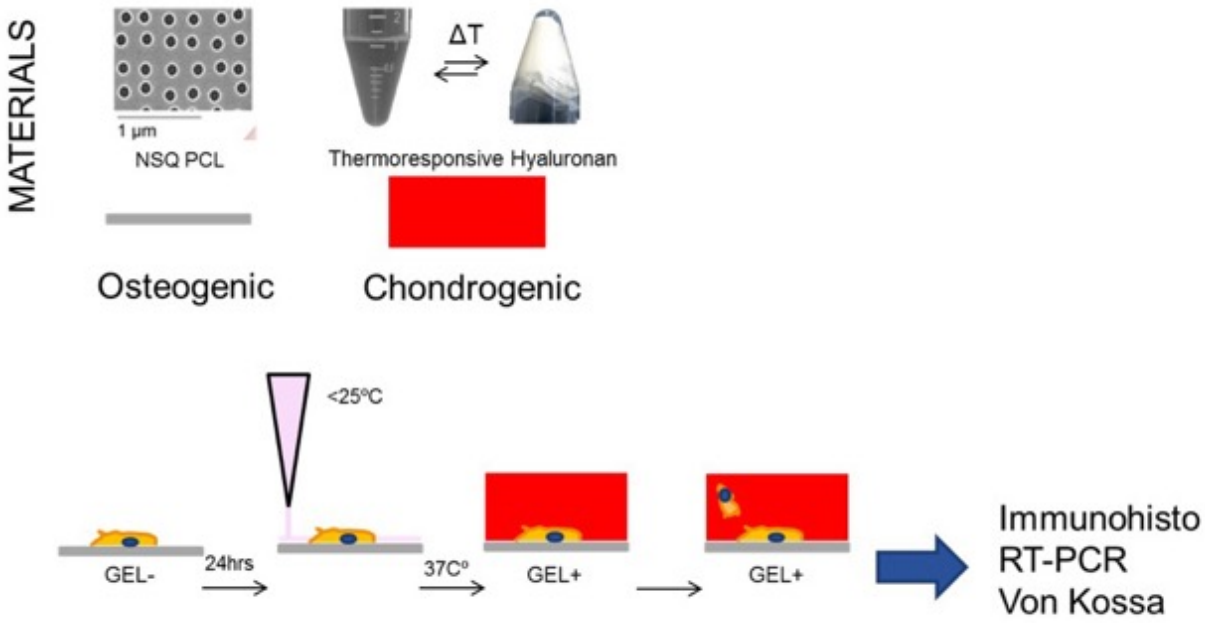

Figure 1. Schematic of basic in vitro experimental set up.

Materials.

Thermoresponsive hyaluronan derivatives formulation used for this study had an average degree of substitution value of 6.42 ± 0.40% as measured by 1H NMR, an

average storage modulus (G') value of 0.46 ±□0.226.7 Pa at 25°C and 1090 ± 6602492 Pa at 35°C.

To assess the influence of hMSCs on the stability and rheological properties of the hydrogel formulation, 20 million hMSCs were seeded encapsulated into 1 ml of hyaluronan derivative reconstituted at 15% w:v in PBS and the rheological profile measured (Figure 2). The gelation temperature was not influenced by the presence of cells, while the final storage modulus value decreased from 6.7 to 4.8 Pa at 25°C and from 1100Pa down to 1000Pa kPa at 35°C.

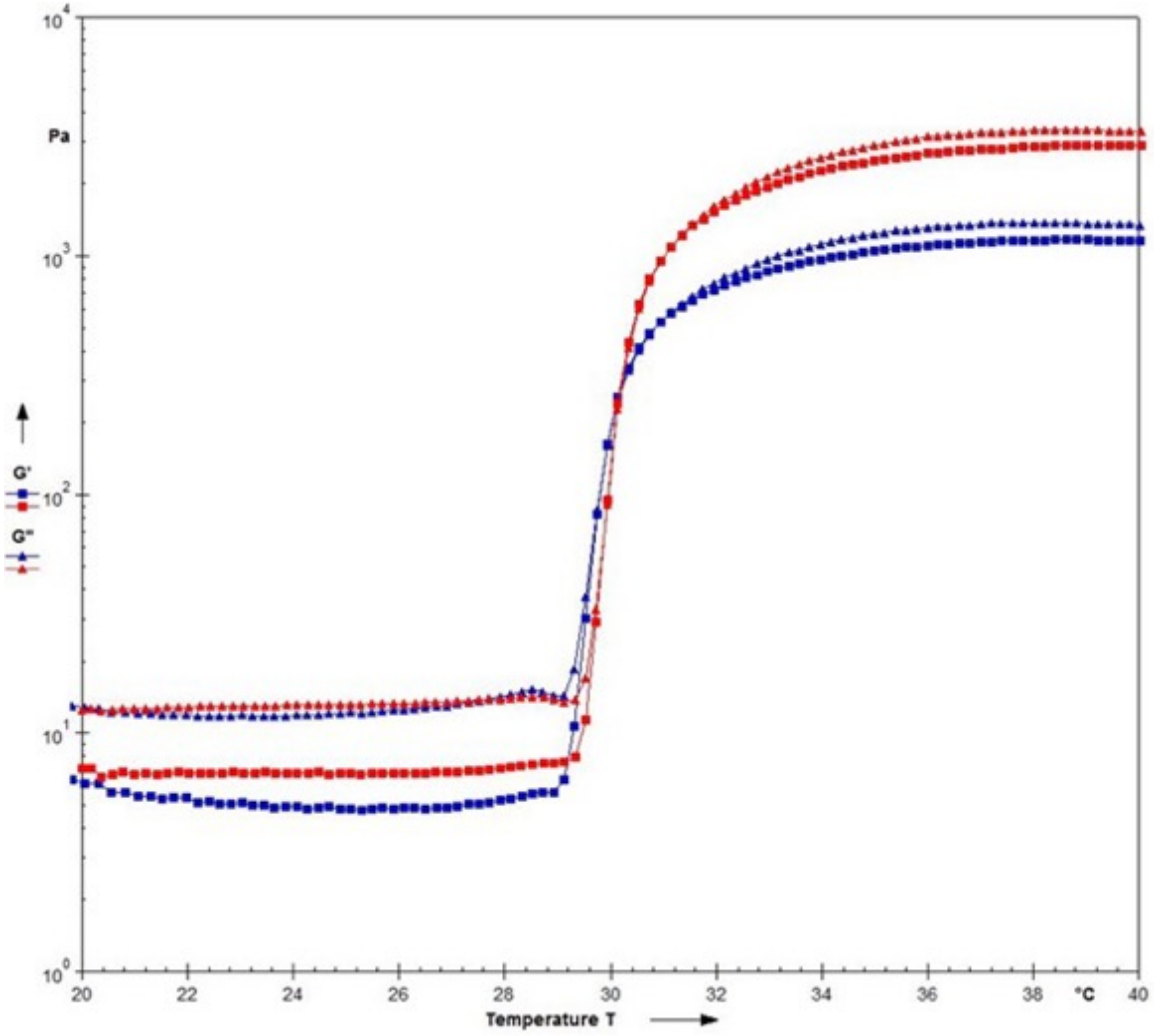

Figure 2. Rheological features of the gel with (blue symbols) and without (red symbols) hMSCs. Cells were seeded at 20 x10^6 cell/ml. Squares represent storage moduli, triangles loss moduli. Cell presence has a minor impact on the rheological properties.

Morphological analysis.

MSCs cultured for 5 days on FLAT or NSQ patterned PCL with and without the addition of the hydrogel were first subject to immunofluorescence microscopy in order to analyse differences in cellular morphology between the different materials. Samples were fluorescently stained for either β3-tubulin or vimentin alongside a nuclear stain. The

FLAT control surfaces exhibited great variation in cellular morphology within samples, with most cells spindle-shaped typical of fibroblast morphologies, alongside more stellate or rounded morphologies more typical of osteogenic or chondrogenic/adipogenic lineages (Figure 3(a) & (b) (tubulin), (g) & (h) (vimentin)). Whereas NSQ surfaces consistently led to well spread, polygonal cells with large nuclei (Figure 4), typical of osteoblastic morphologies (Figure 3(d) & (e) (tubulin), (j) & (k) (vimentin)). More organised tubulin microtubule and vimentin intermediate filament networks were observed in larger, polygonal cells on the NSQ surfaces (Figure 3(d) & (e) (tubulin), (j) & (k) (vimentin)). Within the hyaluronan hydrogel, a small number of cells were observed. Cells in the hydrogel exhibited rounded morphologies of ~ 10-25 μm in diameter typical of chondrogenic morphology, and this was maintained throughout samples regardless of underlying surface topography.

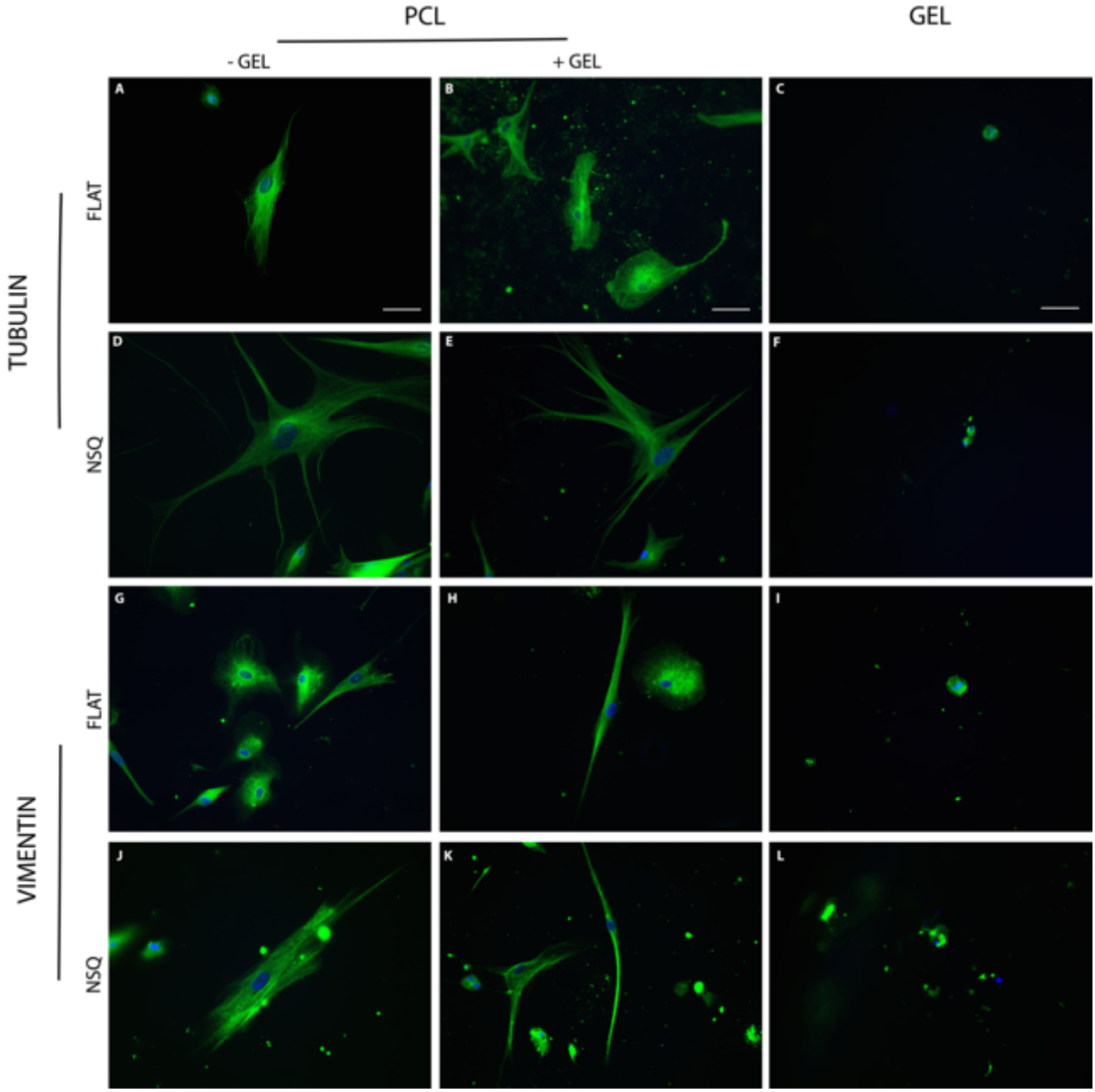

Figure 3. Cytoskeletal morphology analysis of MSCs cultured on FLAT and NSQ topography with and without addition of Hyal hydrogel. Images of immunostained MSCs cultured for 5 days on PCL surfaces of FLAT (A – C, G - I) or NSQ (D – F, J – L) topography, with and without addition of hydrogel. Cells exhibit varied morphology typical of several mesenchymal lineages on FLAT surfaces +/- gel, where NSQ leads to well spread polygonal cells typical of osteoblast morphology. Note rounded morphology, typical of chondrogenesis, in hydrogels cultured with either FLAT or NSQ surfaces. Green is tubulin A – F, vimentin G – L, blue is DAPI nuclear stain. Scale bar is 50 μm.

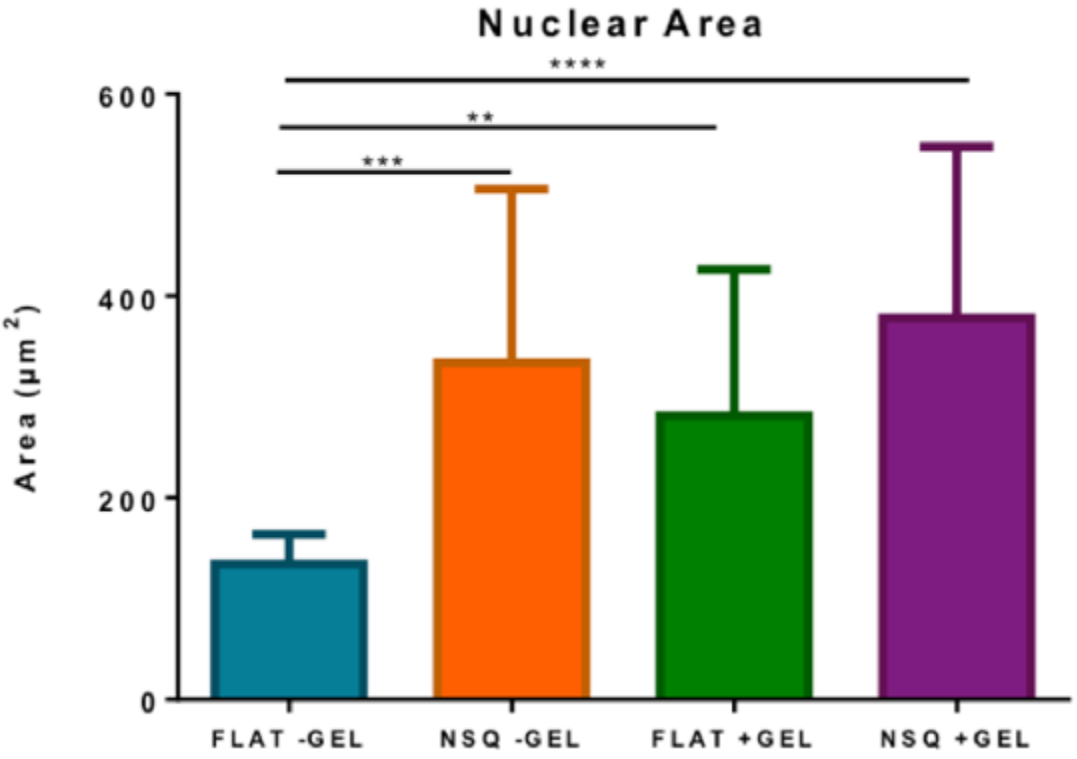

Figure 4. Nuclear area of hMSCs cultured on FLAT +/-GEL and NSQ +/-GEL for 5 days. NSQ topographies consistently lead to a larger nuclear area, indicative of increased cellular spreading associated with osteoblastic morphologies. The change in matrix elasticity upon addition of the hydrogel also led to a lesser yet significant increase in nuclear area on FLAT surfaces. Data presented is mean nuclear area ±SD. Comparison was done by ANOVA **P <0.01, ***P <0.001, ****P <0.0001, n = 20.

Transcription factor expression analysis.

Following analysis of MSC morphology, expression of phosphorylated runt-related transcription factor type 2 (pRUNX2), a marker for osteogenic differentiation, and sex-determining region Y-box 9 (SOX9), a transcription factor involved in chondrogenic differentiation were observed by immunofluorescence microscopy in MSCs cultured for 5 days on FLAT or NSQ patterned PCL with and without the addition of the hydrogel.

RUNX2 expression on FLAT surfaces was abundant in both the nucleus and in the perinuclear region of the cytoplasm (Figure 5(a) & (b)), whereas on NSQ surfaces RUNX2 appears highly abundant in the nucleus with only negligible detection in the

perinuclear region (Figure 5(d) & (e), co-localisation shown as turquoise colour (blue/green overlay)). Also, there were notably larger nuclei observed in the NSQ populations compared with control FLAT populations (more examples of MSC nuclei on NSQ in Sup Figure 2). It should also be noted that RUNX2 is also an indicator of late chondrogenesis [29,30]; and positive RUNX2 expression was detectable in cytoplasm (not in the nuclei) of MSCs that had migrated into the hydrogel regardless of underlying PCL surface topography (Figure 5(c) & (f)).

SOX9 expression was detected on FLAT surfaces at low levels in some cells throughout the sample but was located in the cytoplasm only (Figure 5(g) and (h)). In MSCs on the NSQ surfaces, SOX9 expression was mainly negligible (Figure 5(j) & (k)). Consistent with RUNX2 expression, SOX9 was abundantly present in cells that had migrated into the hydrogels regardless of the underlying PCL surface topography (Figure 5(i) & (l)).

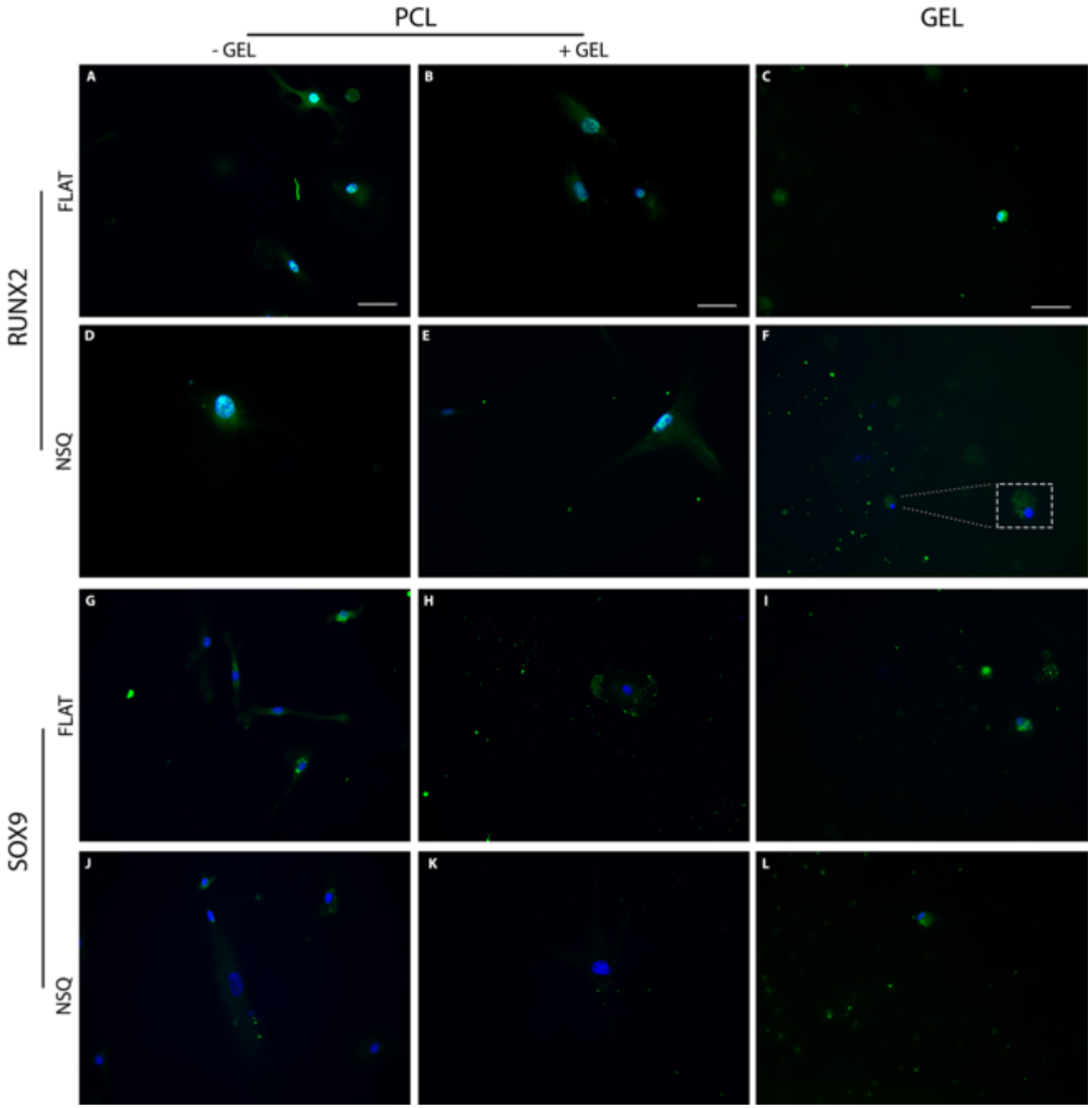

Figure 5. Osteogenic and Chondrogenic transcription factor expression analysis of MSCs cultured on FLAT and NSQ topography with and without addition of Hyal hydrogel. Images of immunostained MSCs cultured for 5 days on PCL of FLAT (A – C, G - I) or NSQ (D – F, J-L) topography, with and without addition of hydrogel. A – F showing osteogenic marker phosphorylated RUNX2 expression, note large nuclear area on NSQ surfaces with high nuclear expression and localisation. Note expression in rounded cells in hydrogel. G – L showing chondrogenic marker SOX9 expression, note cytoplasmic expression in FLAT samples compared to very low levels detected on NSQ, with cells in hydrogels showing clear positive expression. Green is phosphoRUNX2 A – F, SOX9 G – L, blue is DAPI nuclear stain. Scale bar is 50 µm. Turquoise colour (blue/green overlay) = co-localisation.

Matrix maturation and mineralization.

MSCs were cultured on FLAT and NSQ surfaces with and without hydrogel for 28 days and immunofluorescence was used to detect expression of the bone-specific extracellular matrix protein osteocalcin (OCN), an osteoblast differentiation marker. On the FLAT surfaces without gel, only very low levels of OCN were detected (Figure 6(a)). With addition of gels OCN expression increased notably (Figure 6(b)). OCN levels were, however, high on the NSQ samples without the hydrogel (Figure 6(c)) and this expression of OCN increased further with hydrogel addition (Figure 6(d)).

Further to this, MSCs that had been cultured for 28 days were assessed for mineralization via von Kossa staining (stain for calcium deposits present in bone mineral, therefore suggestive of osteogenic differentiation), in which the trend observed was consistent with the immunofluorescence analysis with maximal expression seen in cells cultured on NSQ with gels on top (note that the gel was removed during staining) (Figure 6(e)).

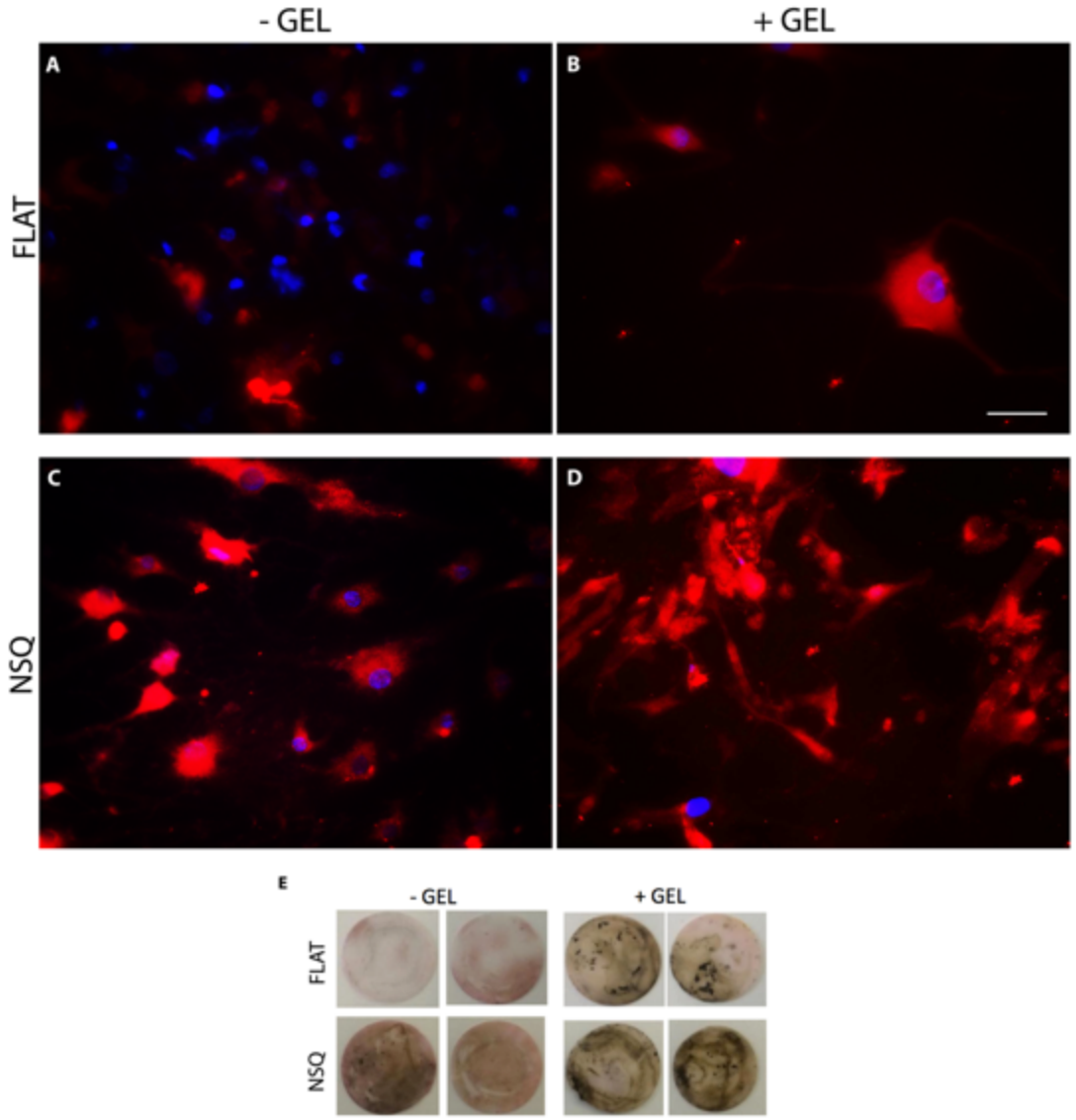

Figure 6. MSC mineralization analysis following long-term culture. A – D. RGB images of immunostained MSCs cultured for 28 days on PCL surfaces with FLAT (A, B) or NSQ (C, D) topography, with (B, D) and without (A, C) addition of hydrogel. Samples were stained for osteocalcin secretion. (E) MSCs cultured on PCL for 28 days and von kossa stained. Note increase in positive staining in all NSQ compared to FLAT, with slight increase also observed on FLAT + gel. Green is osteocalcin, blue is DAPI nuclear stain. Scale bar is 100 µm.

Discussion

The current study investigated the use of a chondropermisive hyaluronan hydrogel in combination with a well-defined topography presented on a biodegradable, biocompatible

polymer as a method to produce a tissue engineered cartilage-bone interface from a single multipotent cell source.

The NSQ topography provides targeted osteogenesis from MSC populations, while the FLAT control surface results in uncontrolled heterogeneous differentiation. This is in agreement with published data.[11] Cells cultured on NSQ consistently had a well-spread, polygonal morphology with notably increased nuclear size in comparison to those cultured on control surfaces. It is now understood that the NSQ arrangement is able to promote osteogenesis by encouraging this well-spread morphology. Through integrin receptor-related signalling[31] and BMP2 signalling[32], RUNX2 is phosphorylated (activated) and thus the transcription of osteoblast specific genes essential for bone homeostasis occurs.[33] Further, changes in nucleus size in cells on NSQ has been implicated in changing chromosomal positioning and hence direct cellular mechanotransduction.[34,25] When cultured with the hydrogel in place, NSQ surfaces continued to direct osteogenesis of MSCs on the surface, whereas FLAT surfaces displayed evidence of an increase in a rounded cell population on the surface. This can be speculated to suggest that cues presented by the hydrogel in 3D culture predominate other mechanical or chemical cues presented by the FLAT surfaces but not the topographical cues presented by the NSQ surfaces. This is perhaps logical as the cell-cell mimicking effects of hyluronan have been previously implicated in chondrogenesis[35], through interaction with the CD44 antigen.

Previous studies have confirmed the viability of culturing MSCs in the hydrogel and also presented strong evidence of chondropromotive environment provided by the hyaluronan based hydrogel[15,36], with a further study investigating the biocompatibility *in vivo*.[37] The

addition of cells to the hydrogel led to a decrease of storage modulus after the transition. This is to be expected, because the gelation mechanism is based on non-covalent interactions prone to disruption by the presence of MSC, especially at such a high concentration. However, the gelation temperature remained unvaried and the cell-containing hydrogel underwent a >200-fold increase of storage modulus in a very narrow temperature window. In agreement with the previous findings, we found cells cultured in the hydrogel were consistently rounded, typical of chondrocyte morphology with clear expression of chondrogenic marker SOX9. Although not statistically significant, due to a large volume of hydrogel and small volume of cells introducing variability, gene expression analysis shows SOX9 detection in the gel (supplementary figure 3). It is suggested that the lack of degradation sensitive sites presented in the hydrogel network restricts cellular spread, promoting this rounded morphology and thus directing chondrogenic differentiation.[3,15] Further, there is a lack of integrin specific ligands in the gel. In the same study, hMSCs cultured in the hydrogel underwent chondrogenic differentiation even when cultured in osteogenic media.[15] It is noteworthy that HA is a native component of cartilage and as indicated in this, and previous studies, it may be responsible for maintaining the chondrocyte phenotype.

When considering orthopaedic applications of the construct, injection of the hydrogel into subchondral defects in rabbit highlighted clinical transferability of the gel itself. In the study by D'Este, *et al*., 2016, biocompatibility and ease of use was confirmed, as the gel was injected into the site of the defect. Gel shearing from the nanotopographical surface could present a potential limitation of this construct upon scaling-up. However, the 2016

study validated retention of the gel in a partially weight-bearing osteochondral defect within a moving synovial joint for up to 12 weeks; it was also noted here that the implanted gels had lost their reversibility upon long-term harvesting.[37]

This study highlights that differential tuning of the extracellular environments chemical, physical and mechanical properties can lead to the targeted differentiation of cells down different tissue lineages within the same culture. Two materials were used for *in vitro* culture of MSCs, both of which have previously been fully characterized.[5,15] Here, we introduce the possibility to create interfaces capable of directing anisotropic cell and potentially tissue growth, which can have important implications in complex tissue engineering. Analysis confirmed that when put together, the materials retained their abilities to direct differentiation down two distinct lineages, as expected, NSQ topography consistently led to osteogenesis and we were able to confirm targeted chondrogenesis of cells that migrated from the surface into the hydrogel. This novel system combines two simple materials with different differentiation capacities and cells from a single source to create a platform with the capability to sustain the growth of two tissue types in culture. This proof-of-concept system highlights that multi-compartmental material systems that control spatial differentiation of MSCs can be made, but the current system is perhaps more suited to drug testing than orthopaedic use due to its mechanical characteristics that need to be developed. It is envisioned that creating more biomimetic grafts through complex tissue engineering techniques as such could be exploited to improve success of current approaches.

Acknowledgements

We thank the AO Foundation for grant S-12-01M. We also acknowledge the support of EPSRC project EP/K034898/1 and the European Research Council Starting Grant STROFUNSCAFF.

References

1. Oldershaw R a. Cell sources for the regeneration of articular cartilage: The past, the horizon and the future. *Int J Exp Pathol* 2012; 93: 389–400.
2. Benoit DSW, Schwartz MP, Durney AR, et al. Small functional groups for controlled differentiation of hydrogel-encapsulated human mesenchymal stem cells. *Nat Mater* 2008; 7: 816–23.
3. Engler AJ, Sen S, Sweeney HL, et al. Matrix elasticity directs stem cell lineage specification. *Cell* 2006; 126: 677–89.
4. McMurray RJ, Gadegaard N, Tsimbouri PM, et al. Nanoscale surfaces for the long-term maintenance of mesenchymal stem cell phenotype and multipotency. *Nat Mater* 2011; 10: 637–44.
5. Cassidy JW, Roberts JN, Smith C-A, et al. Osteogenic lineage restriction by osteoprogenitors cultured on nanometric grooved surfaces: the role of focal adhesion maturation. *Acta Biomater* 2014; 10: 651–60.
6. Dalby MJ, Gadegaard N, Tare R, et al. The control of human mesenchymal cell differentiation using nanoscale symmetry and disorder. *Nat Mater* 2007; 6: 997–1003.
7. Mata A, Kim EJ, Boehm CA, et al. A three-dimensional scaffold with precise micro-architecture and surface micro-textures. *Biomaterials* 2009; 30: 4610–4617.
8. Morrison SJ, Shah NM, Anderson DJ. Regulatory mechanisms in stem cell biology. *Cell* 1997; 88: 287–298.
9. Mata A, Hsu L, Capito R, et al. Micropatterning of bioactive self-assembling gels. *Soft Matter* 2009; 5: 1228–1236.
10. Mendes AC, Smith KH, Tejeda-Montes E, et al. Co-assembled and microfabricated bioactive membranes. *Adv Funct Mater* 2013; 23: 430–438.
11. Fei D, Ker E, Chu B, et al. Engineering Spatial Control of Multiple Differentiation Fates within a Stem Cell Population. *Biomaterials* 2011; 32: 3413–3422.
12. Re'Em T, Witte F, Willbold E, et al. Simultaneous regeneration of articular cartilage and subchondral bone induced by spatially presented TGF-beta and BMP-4 in a bilayer affinity binding system. *Acta Biomater* 2012; 8: 3283–3293.
13. Chen J, Chen H, Li P, et al. Simultaneous regeneration of articular cartilage and subchondral bone in vivo using MSCs induced by a spatially controlled gene

delivery system in bilayered integrated scaffolds. *Biomaterials* 2011; 32: 4793–4805.

14. Yin Z, Zhang L, Wang J. Repair of articular cartilage defects with 'two-phase' tissue engineered cartilage constructed by autologous marrow mesenchymal stem cells and 'two-phase' allogeneic bone matrix gelatin. *Zhongguo Xiu Fu Chong Jian Wai Ke Za Zhi* 2005; 19: 652–657.
15. Seelbach RJ, Fransen P, Peroglio M, et al. Multivalent dendrimers presenting spatially controlled clusters of binding epitopes in thermoresponsive hyaluronan hydrogels. *Acta Biomater* 2014; 10: 4340–50.
16. D'Este M, Alini M, Eglin D. Single step synthesis and characterization of thermoresponsive hyaluronan hydrogels. *Carbohydr Polym* 2012; 90: 1378–85.
17. Yang X, Tare RS, Partridge K a, et al. Induction of human osteoprogenitor chemotaxis, proliferation, differentiation, and bone formation by osteoblast stimulating factor-1/pleiotrophin: osteoconductive biomimetic scaffolds for tissue engineering. *J Bone Miner Res* 2003; 18: 47–57.
18. Lathia JD, Okun E, Tang S-C, et al. Toll-Like Receptor 3 Is a Negative Regulator of Embryonic Neural Progenitor Cell Proliferation. *J Neurosci* 2008; 28: 13978–13984.
19. Wang Z, Sugano E, Isago H, et al. Differentiation of neuronal cells from NIH/3T3 fibroblasts under defined conditions. *Dev Growth Differ* 2011; 53: 357–365.
20. Dalby MJ, Biggs MJP, Gadegaard N, et al. Nanotopographical stimulation of mechanotransduction and changes in interphase centromere positioning. *J Cell Biochem* 2007; 100: 326–38.
21. Tetsunaga T, Nishida K, Furumatsu T, et al. Regulation of mechanical stress-induced MMP-13 and ADAMTS-5 expression by RUNX-2 transcriptional factor in SW1353 chondrocyte-like cells. *Osteoarthr Cartil* 2011; 19: 222–232.
22. Kilian K a, Bugarija B, Lahn BT, et al. Geometric cues for directing the differentiation of mesenchymal stem cells. *Proc Natl Acad Sci U S A* 2010; 107: 4872–7.
23. Nikukar H, Reid S, Tsimbouri PM, et al. Osteogenesis of mesenchymal stem cells by nanoscale mechanotransduction. *ACS Nano* 2013; 7: 2758–67.
24. Rico P, Mnatsakanyan H, Dalby MJ, et al. Material-Driven Fibronectin Assembly Promotes Maintenance of Mesenchymal Stem Cell Phenotypes. 2016; 6563–6573.
25. Tsimbouri PM, Murawski K, Hamilton G, et al. A genomics approach in determining nanotopographical effects on MSC phenotype. *Biomaterials* 2013; 34: 2177–2184.
26. Medvedev SP, Grigor'eva E V, Shevchenko AI, et al. Human Induced Pluripotent Stem Cells Derived from Fetal Neural Stem Cells Successfully Undergo Directed

Differentiation into Cartilage. *Stem Cells Dev* 2011; 20: 1099–1112.

27. Llopis-hernández V, Cantini M, González-garcía C, et al. Material-driven fibronectin assembly for high-efficiency presentation of growth factors. *Sci Adv* 2016; 1–11.
28. Livak KJ, Schmittgen TD. Analysis of relative gene expression data using real-time quantitative PCR and the 2(-Delta Delta C(T)) Method. *Methods* 2001; 25: 402–8.
29. Enomoto H, Furuichi T, Zanma A, et al. Runx2 deficiency in chondrocytes causes adipogenic changes in vitro. *J Cell Sci* 2004; 117: 417–425.
30. Stricker S, Fundele R, Vortkamp A, et al. Role of Runx genes in chondrocyte differentiation. *Dev Biol* 2002; 245: 95–108.
31. Tsimbouri PM, McMurray RJ, Burgess K V, et al. Using nanotopography and metabolomics to identify biochemical effectors of multipotency. *ACS Nano* 2012; 6: 10239–49.
32. Yang J, McNamara LE, Gadegaard N, et al. Nanotopographical Induction of Osteogenesis through Adhesion, Bone Morphogenic Protein Cosignaling, and Regulation of MicroRNAs. *ACS Nano* 2014; 8: 9941–9953.
33. Ge C, Xiao G, Jiang D, et al. Critical role of the extracellular signal-regulated kinase-MAPK pathway in osteoblast differentiation and skeletal development. *J Cell Biol* 2007; 176: 709–718.
34. Tsimbouri P, Gadegaard N, Burgess K, et al. Nanotopographical effects on mesenchymal stem cell morphology and phenotype. *J Cell Biochem* 2014; 115: 380–390.
35. Marklein RA, Burdick JA. Controlling stem cell fate with material design. *Adv Mater* 2010; 22: 175–189.
36. Peroglio M, Eglin D, Benneker LM, et al. Thermoreversible hyaluronan-based hydrogel supports in vitro and ex vivo disc-like differentiation of human mesenchymal stem cells. *Spine J* 2013; 13: 1627–39.
37. D'Este M, Sprecher CM, Milz S, et al. Evaluation of an injectable thermoresponsive hyaluronan hydrogel in a rabbit osteochondral defect model. *J Biomed Mater Res - Part A* 2016; 104: 1469–1478.